Zoosyst. Evol. 101 (4) 2025, 2191–2205 | DOI 10.3897/zse.101.164102

First records of *Bathytoshia brevicaudata* (Hutton, 1875) (Myliobatiformes, Dasyatidae) from China with mitogenomic evidence

Jia-Jie Chen[1,2*], Jiang-Yuan Chen[1,3*], Xing-Le Guo[4], Sheng Zeng[5], De-Yuan Yang[5,6], Jun-Sheng Zhong[2], Shen-Long Zhao[7], Wen-Hong Fang[1*], Jian Chen[7*], Pan Liu[8*]

1 *East China Sea Fisheries Research Institute, Fisheries Science of Chinese Academy, 200090, Shanghai, China*
2 *Shanghai Universities Key Laboratory of Marine Animal Taxonomy and Evolution, Shanghai Ocean University, 201306, Shanghai, China*
3 *Fisheries College, Ocean University of China, Qingdao 266003, China*
4 *Laboratory of Fisheries Ecology and Biodiversity, College of Fisheries, Zhejiang Ocean University, Zhoushan 316022, China*
5 *College of the Environment and Ecology, Xiamen University, 361102, Xiamen, China*
6 *National Taiwan Ocean University, Keelung, 202301, Taiwan, China*
7 *Marine Science and Technology College, National Engineering Laboratory of Marine Germplasm Resources Exploration and Utilization, Zhejiang Ocean University, Zhoushan 316022, China*
8 *Conversation and Research Center for Collections, Shanghai Natural History Museum, Branch of Shanghai Science and Technology Museum, 200041, Shanghai, China*

https://zoobank.org/05A33FE9-5BF1-4C9F-8432-92E172DF5DEA

Corresponding authors: Wen-Hong Fang (fwenhong@163.com); Jian Chen (chenjian@zjou.edu.cn) Pan Liu (liup@sstm.org.cn)

Academic editor: Nalani Schnell ♦ **Received** 4 July 2025 ♦ **Accepted** 16 October 2025 ♦ **Published** 17 November 2025

Abstract

This study presents the first records of the Broad-tail Stingray, *Bathytoshia brevicaudata* (Hutton, 1875), in the East China Sea, significantly extending its known distribution in the Northwest Pacific. Through comprehensive morphological examination of male and female specimens, we identified several sexually dimorphic traits, including the number of oral papillae rows, dorsal tubercle spines, and tooth cusp morphology. Stomach content analysis revealed predation on teleosts exceeding 30 cm total length, challenging previous dietary descriptions. Furthermore, the co-occurrence of distinct fishing hook types (coastal J-hook and pelagic circle hook) within one specimen provides empirical evidence of transboundary movements between neritic and oceanic zones. We also sequenced and characterized the complete mitogenomes of both sexes (17,640 bp; GenBank: PV699610–PV699611), which exhibited conserved dasyatid genomic features, including pronounced AT bias (59.2%), purifying selection across protein-coding genes (strongest in *cox2*), and structural traits such as an incomplete stop codon in *ND4* and a DHU-arm-deficient *trnS1*. These integrative findings enhance the ecological and molecular understanding of *B. brevicaudata* and provide critical baseline data for its conservation in poorly studied regions of the Indo-Pacific.

Key Words

Hainan Island, mitochondrial genome, phylogenetic analysis, South China Sea, taxonomic key

* These authors contributed equally to this work.

Copyright *Chen, J.-J. et al.* This is an open access article distributed under the terms of the Creative Commons Attribution License (CC BY 4.0), which permits unrestricted use, distribution, and reproduction in any medium, provided the original author and source are credited.

Introduction

Bathytoshia Whitley, 1933, is a widely distributed genus in temperate Atlantic and Indo-West Pacific waters that has long been taxonomically disputed regarding its species composition. Current consensus recognizes three valid species: *B. centroura* (Mitchill, 1815) in the Atlantic, and *Bathytoshia brevicaudata* (Hutton, 1875) and *B. lata* (Garman, 1880) occurring in the northwestern Pacific, among other regions (Last et al. 2016a, 2016b).

The type locality of *Bathytoshia brevicaudata* is in New Zealand (Hutton 1875) and the species exhibits a disjunct distribution, divided by tropical seas into three isolated regions: the coastal waters of southern Africa, southern Australia-New Zealand, and the temperate northwestern Pacific (Last et al. 2016b). Due to the vast geographical separation between the northern and southern populations, the northwestern Pacific population was historically regarded as a distinct species, *Dasyatis matsubarai* (Miyoshi, 1939) (Miyosi 1939). However, subsequent morphological and molecular studies have relegated *D. matsubarai* to a junior synonym of *B.brevicaudata* (Le Port et al. 2013). Recent records include its first occurrence in southern Japan (Takushi et al. 2025) and South Korea (Kim et al. 2020). These recent records reported its complete mitochondrial genome sequence without detailed characterizing. Biological and ecological knowledge of this species remains limited.

Studies on *Bathytoshia* spp. remain limited in China, with only *B. lata* having been historically recorded from Chinese waters (Zhu and Meng 2001; Wu and Zhong 2021). *B. brevicaudata* distribution was considered restricted to East coast waters of Taiwan Island, recorded as a specimen (FRIP20268; catalog 0268; 22.06°N, 121.51°E; http://catalog.digitalarchives.tw/item/00/26/49/f9.html) caught near Lanyu Island in 1987, originally identified as *Dasyatis matsubarai* (793 mm TL). However, this specimen likely represents *Pteroplatytrygon violacea* (Bonaparte, 1832) based on photographic evidence showing a purple-black dorsum and absent pectoral fin spots. No other Chinese records of *B. brevicaudata* exist, yet field surveys document abundant *B. lata* (1.2–1.5 m disc width, 200–300 kg) numbers in trawl catches at Taizhou, Zhejiang (Suppl. material 1: fig. S1) and Xiamen, Fujian of East China Sea and the Taiwan Strait (Suppl. material 1: fig. S2). We hypothesize that unreported *B. brevicaudata* populations may exist due to confusion between these large, broad stingrays.

In this study, we report the first formal records of *B. brevicaudata* from the open water of northern Zhejiang, East China Sea, based on two voucher specimens (♂ ZJOUMBM F00035; ♀ ECSFRI 28263), and provide detailed morphological descriptions. We conducted dissection and qualitative stomach content analysis of the female specimen. We also sequenced, annotated, and characterized complete mitogenomes of the specimens with comparative analysis against Korean conspecifics (Kim et al. 2020), and reconstructed a myliobatiform phylogeny using mitogenomes from 52 species to elucidate their evolutionary relationships.

Materials and methods

Sample collection, morphological examination, and DNA extraction

Two specimens of *Bathytoshia brevicaudata*, comprising a mature male (voucher ZJOUMBM F00035, 42 kg, Fig. 1, Suppl. material 1: fig. S3) and a mature female (voucher ECSFRI 28263, 60 kg, Fig. 2, Suppl. material 1: fig. S4), were collected as bycatch during bottom trawling in the East China Sea in March 2025. The specimens were landed at Songmen Port, Zhejiang Province, China. Subsequently, our team performed morphological measurements and tissue sampling on the specimens. Methods for measurements followed Compagno and Roberts (1982). Radial cartilage counts were obtained through dissection during the preparation of stripped specimens. An approximately 5 × 5 mm^2 block of muscle tissue, which had been preserved in 100% ethanol, was clipped below the ventral dorsal fin of the specimens for DNA extraction. Whole genomic DNA was extracted using the TIANamp Genomic DNA kit (TIANGEN, Beijing, China).

The two specimens are deposited at the Zhejiang Ocean University Museum of Marine Biodiversity (ZJOUMBM) and East China Sea Fisheries Research Institute (ECSFRI), respectively. The male individual was preserved in 10% neutral buffered formalin, while the female specimen underwent systematic biological dissection followed by taxidermy preparation.

The stomach contents of the dissected female specimen (ECSFRI 28263) are deposited at the Shanghai Natural History Museum (SHNHM, voucher SNHM-Hfi13442, 95% ethanol), while its stomach and liver remain preserved at ECSFRI (voucher 28366~28367, in 10% neutral buffered formalin). Measurement of fishing hooks in stomach contents followed the standard protocols of Alós (2008) and Swimmer et al. (2010).

Mitogenome sequencing and assembly

The mitochondrial genomes were sequenced and assembled following established protocols (Chen et al. 2024; Xu et al. 2024; Yang et al. 2024). DNA libraries were prepared with the Illumina TruSeqTM DNA Sample Preparation Kit (Illumina, USA) following manufacturer guidelines. Novogene Bioinformatics Technology Co., Ltd. (China) conducted sequencing on a DNBSEQ-T7 platform, generating 150 bp paired-end reads yielding ~5 Gb raw data per sample. Data preprocessing involved Fastp v0.23.2 (Chen et al. 2018) with default parameters and quality assessment using FastQC v0.12.1 (http://www.bioinformatics.babraham.ac.uk/projects/fastqc/). Mitogenome assembly employed the FastMitoAssembler pipeline, augmented by GetOrganelle v1.7.6.1 (Jin et al. 2020) and NovoPlasty v4.3.1 (Dierckxsens et al. 2017).

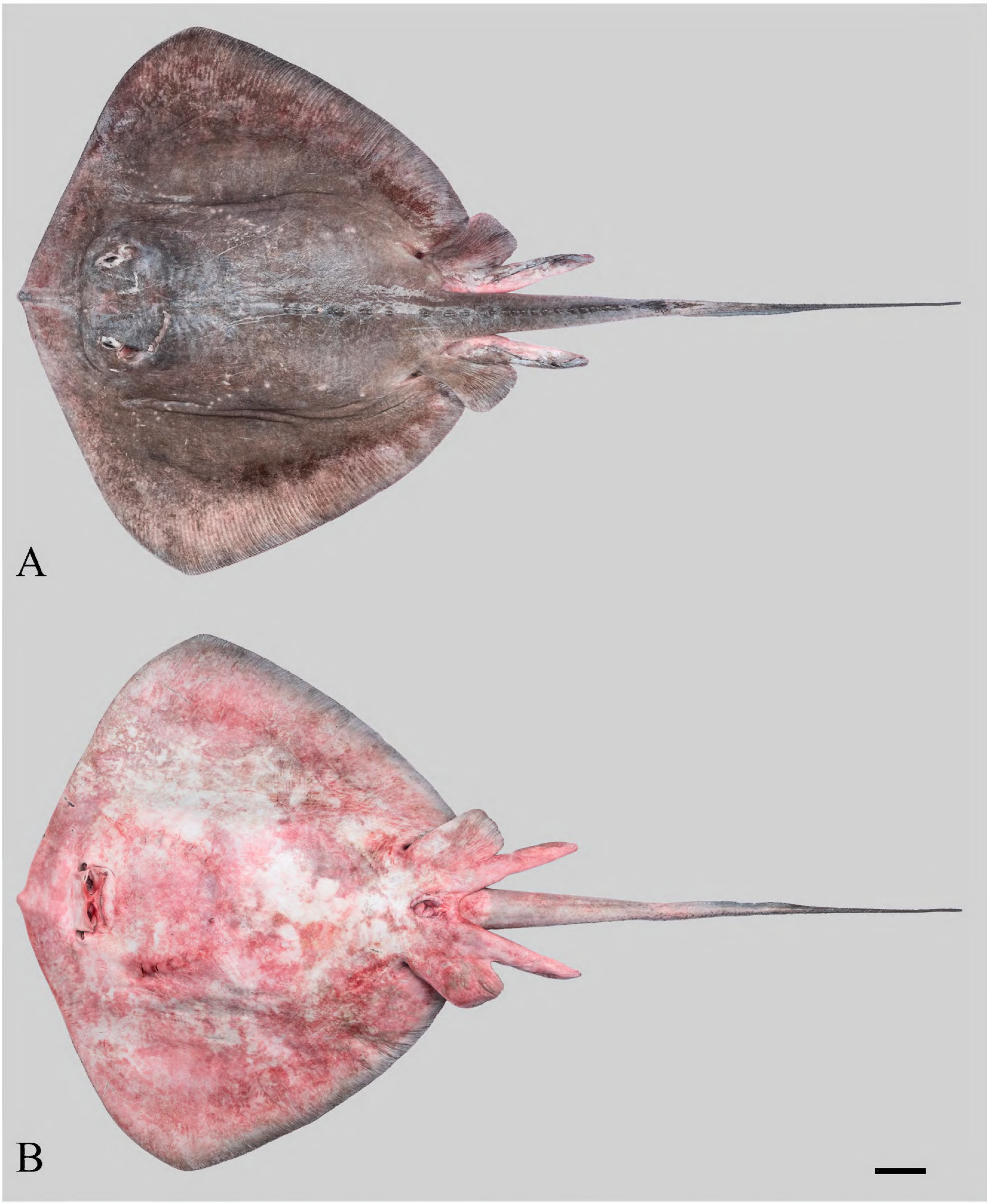

Figure 1. Dorsal (**A**) and ventral (**B**) view of *Bathytoshia brevicaudata*, ZJOUMBM F00035, male, photo by Rui-Lin Huang.

Mitogenome annotation and sequence analyses

The complete mitochondrial genome was annotated using MITOS2 (Donath et al. 2019) and Mitoz v3.6 (Meng et al. 2019), with manual validation in Geneious v2021.0.3. PhyloSuite v1.2.3 (Zhang et al. 2020) was employed to quantify base composition, codon usage, and relative synonymous codon usage (RSCU) of protein-coding genes (PCGs). Nucleotide skewness (A+T skew = [A%−T%]/[A%+T%]; G+C skew = [G%−C%]/[G%+C%]) was calculated following Perna and Kocher (1995). Selective pressure analysis through Ka/Ks ratios was conducted for Dasyatinae species mitogenomes using DnaSP 6.0 (Rozas et al. 2017). Transfer RNA secondary structures predicted by tRNAscan-SE 2.0 (Lowe and Chan 2016; Chan et al. 2021) and MITOS (Bernt et al. 2013) were visualized

Figure 2. Dorsal (**A**) and ventral (**B**) view of *Bathytoshia brevicaudata*, ECSFRI 28263, female, photo by Rui-Lin Huang.

through ViennaRNA Web Services (Kerpedjiev et al. 2015; http://rna.tbi.univie.ac.at/forna/). The complete mitogenome sequences of the two specimens were ultimately determined and deposited in NCBI under accession numbers PV699610 (voucher ECSFRI 28263, female) and PV699611 (voucher ZJOUMBM F00035, male).

Phylogenetic analysis

We reconstructed the myliobatiform phylogeny using mitogenomes from 52 species, with *Narcine timlei* (Bloch & Schneider, 1801) and *Rhinobatos schlegelii* Müller & Henle, 1841 designated as outgroups. Mitogenome sequences retrieved from GenBank (Suppl. material 1: table S1) were processed in PhyloSuite 1.2.3 (Zhang et al. 2020). Thirteen protein-coding genes (PCGs) were aligned codon-wise using MAFFT v7.313 (Katoh and Standley 2013), and the resulting alignments were trimmed to the length of the shortest sequence to ensure consistent data length. Based on these alignments, pairwise genetic distances (p-distance) were calculated in MEGA X (Kumar et al. 2018), reporting the number of comparisons, mean, and standard deviation for each group. The pairwise p-distance matrices for the genus *Bathytoshia* are provided in Suppl. material 1: table S6. Subsequently, ambiguous regions were further trimmed using Gblocks v0.91 (Castresana 2000). ModelFinder v.2.2.0 (Kalyaanamoorthy et al. 2017) was used to select the best substitution models under the Bayesian Information Criterion (BIC) for maximum likelihood (ML) analysis and the corrected Akaike Information Criterion (AICc) for Bayesian inference (BI) analysis (Suppl. material 1: table S2).

Maximum likelihood analysis used IQ-TREE v2.2.2 with edge-linked partitioning (5,000 ultrafast bootstrap replicates), while Bayesian inference was done using MrBayes v3.2.7a (two parallel runs; 2×10^6 generations) (Ronquist et al. 2012). Final topologies were visualized using iTOL v6 (Letunic and Bork 2016).

Results

Species description

Bathytoshia brevicaudata (Hutton, 1875)

Diagnosis. Large, plain-colored stingray with broad rhombic disc, short snout; dorsal surface greyish-brown, ventral surface whitish with grey margins; oblique white spots and paired anterolaterally-directed white pores at pectoral-fin bases dorsally; pelvic fins small; tail dusky, midline preceding caudal sting bearing row of spear-shaped or star-based thorns and tubercles, post-sting portion blackish distally and covered with sharp thornlets.

Description. Based on 2 specimens, 1,810–1,955 mm TL. Proportional measurements and counts are given in Table 1.

Body large and flattened but thick, with a broad rhombic disc (Figs 1, 2). Disc width 1.2 (female)–1.4 (male) times its length (Table 1). Back smooth with large backward-pointing tubercles (9 in male, 3 in female); tail midline with similar tubercles extending anterior to caudal sting (Figs 1, 2). Snout short and blunt, length 0.22–0.23 times disc length, with irregularly distributed upright tubercles bearing blunt stellate bases, clustered discontinuously between snout tip and anterior orbital margins (Fig. 3A, B). Eyes small, length of orbit and spiracle 2.2 times (male) and 2.7/1.7 times (female) of snout length; interorbital space broad, up to 6 times orbit length (Table 1).

Pectoral fins broad; anterior margins nearly straight; distal apex narrowly rounded; posterior margins smoothly convex; posterior insertion deeply notched; posterior angle bluntly pointed. Pectoral insertions slightly exceeding interorbital width. Pelvic fin origin slightly anterior to pectoral insertion; extending posteriorly beyond pectorals; anterior margin and lateral margins nearly straight, lateral and posterior angles smoothly rounded; pelvic insertion deeply notched (Figs 1, 2). Claspers (male) moderately elongate, length 0.24 times tail length; tips not reaching caudal sting (Table 1).

Tail stout and tapered (not whip-like), short to moderately elongate, length 0.8–1.0 times disc width (males 0.8, females 1.0, estimated); base broad and depressed, width 1.4–1.6 times depth (Table 1); single caudal sting positioned midway, immediately posterior to dorsal thorn row comprising 15 densely arranged enlarged thorns with sharp-tipped projections from base (male) or 7 sparsely spaced thorns (female) (Fig. 3C, D); lateral serrated thorns upright, blunt, stellate-based, numerous, extending to tip; minute thorns densely cover dorsal surface from posterior to caudal sting, extending to terminus; ventral fold distinct (Fig. 3E, F), moderately long (0.3 times tail length) (Table 1), originating slightly posterior to caudal sting origin, extending toward tip but falls far of terminus; dorsal fold degenerated (Fig. 3E, F).

Labial furrows deep; lower jaw weakly convex. Nasal curtain square-shaped, very broad, with margin fringed; nostrils oval, oblique (Fig. 4A, B). Mouth small (Figs 1, 2); floor of mouth with transverse series of 5 (female) or 7 (male) oral papillae; midregion with 3 (male) or 4 (female) prominent elongated papillae, lateral papillae shorter, 1–2 per side (Fig. 4C, D). Teeth small, granular, with 31 (male) and 33 (female) rows on upper jaws, and 34 (male) and 37 (female) rows on lower jaws, arranged in an interlocking pavement pattern. Upper and lower teeth similar, with sharp cusps in male while rounded in female (Fig. 4C, D).

The male specimen ZJOUMBM F00035 possesses claspers measuring 257 mm in length, situated on the posteromedial aspect of the pelvic fins (Suppl. material 1: fig. S5). The dorsal surface of the claspers exhibit a slate-gray coloration, while the ventral surface appears pinkish due to subcutaneous hemorrhaging, with a seminal groove on the dorsal side. The claspers are robust, rigid, and exhibit a fully calcified structure, confirming the adult status of the specimen.

Color. Dorsal surface pale grey, darkest above eyes and on tail tip, with 26–30 (female) or 21–24 (male) white pores arranged diagonally from pectoral fin bases toward pectoral fin leading edges; spiracles white internally; lateral head-encircling pore rows white; disc margin grey; ventral surface white (Figs 1, 2).

To aid in the morphological identification of genus *Bathytoshia*, we propose the following diagnostic key, building upon the taxonomic framework of Last et al. (2016b):

1 Labial furrow deep; pores around side of head and anterior disc white; tail short, usually shorter than disc width .... *B. brevicaudata* (Japan, Australia, New Zealand, southern Africa)
– Labial furrow weak; pores around side of head and anterior disc without prominent color; tail long, longer than disc width 2
2 Mouth usually with 6 oral papillae; tail length 1.6–1.8 times disc width..... *B. centroura* (western Atlantic)
– Mouth with 3–5 oral papillae; tail length about 2 times disc width..... *B. lata* (Indo-western Pacific, eastern Atlantic)

Feeding habits. Dissection of the female specimen revealed stomach contents (Fig. 5) comprising fragmentary prey remains, specifically two *Branchiostegus japonicus* (Houttuyn, 1782) (Horsehead Tilefish), one *Trachurus japonicus* (Temminck & Schlegel, 1844) (Japanese Jack Mackerel), one *Neobythites* Goode & Bean, 1885 sp., and three longline fishhooks. The hooks included one circle hook (front length (FL) 20.2 mm, width (WD) 25.0 mm, gap (GP) 12.4 mm, shaft length (SL) 38.7 mm, offset 10°) piercing the gastric wall into the liver (Suppl. material 1: figs S6, S7) and two J hooks (FL 17.8 mm, WD 17.8 mm, GP 15.2 mm, SL 42.6 mm) lodged within the stomach lumen.

Mitochondrial genomic structure and base composition

The complete mitogenome sequences of two *B. brevicaudata* specimens (PV699610 and PV699611) were both 17,640 bp long, consistent with known Dasyatinae and

Table 1. Measurements and counts data for *Bathytoshia brevicaudata* from China.

Proportional measurements	ZJOUMBM F00035 (male)		ECSFRI 28263 (female)	
	Absolute measurements (mm)	Percentages of disc width (%DW)	Absolute measurements (mm)	Percentages of disc width (%DW)
Total length	1,810	170.75	1,955	150.97
Disc length	868	81.89	1,070	82.63
Head length	428	40.38	525	40.54
Disc width	1,060	100.00	1,295	100.00
Disc depth	145	13.68	176	13.59
Eyeball	26	2.45	29	2.24
Cornea	19	1.79	13	1.00
Interorbital width	160	15.09	180	13.90
Spiracle	61	5.75	63	4.86
Interspiracular width	158	14.91	210	16.22
Nasal curtain	53	5.00	59	4.56
Internarial width	122	11.51	150	11.58
Mouth width	100	9.43	114	8.80
1st gill slit	35	3.30	43	3.32
5th gill slit	22	2.08	31	2.39
Width between 1st gill slits	232	21.89	280	21.62
Width between 5th gill slits	160	15.09	190	14.67
Snout tip to eye	195	18.40	270	20.85
Snout tip to nostril	148	13.96	188	14.52
Snout tip to mouth	195	18.40	240	18.53
Snout tip to 1st gill slit	297	28.02	374	28.88
Snout tip to 5th gill slit	423	39.91	502	38.76
Snout tip to pelvic fin	768	72.45	955	73.75
Snout tip to vent	806	76.04	990	76.45
Pectoral fin inner margin	142	13.40	145	11.20
Pelvic fin anterior margin	192	18.11	180	13.90
Pelvic fin posterior margin	68	6.42	85	6.56
Pelvic fin base	122	11.51	99	7.64
Span of pelvic fins	131	12.36	200	15.44
Clasper length	257	24.25	——	——
Tail length	1,077	101.60	910 (broken)	70.27 (broken)
Tail base width	116	10.94	98	7.57
Tail base depth	71	6.70	72	5.56
Tail fold length	356	33.58	380	29.34
Counts:				
Oral papillae	7		5	
Tooth rows, upper jaw	31		33	
Tooth rows, lower jaw	34		37	
Total pectoral radials	——		123	

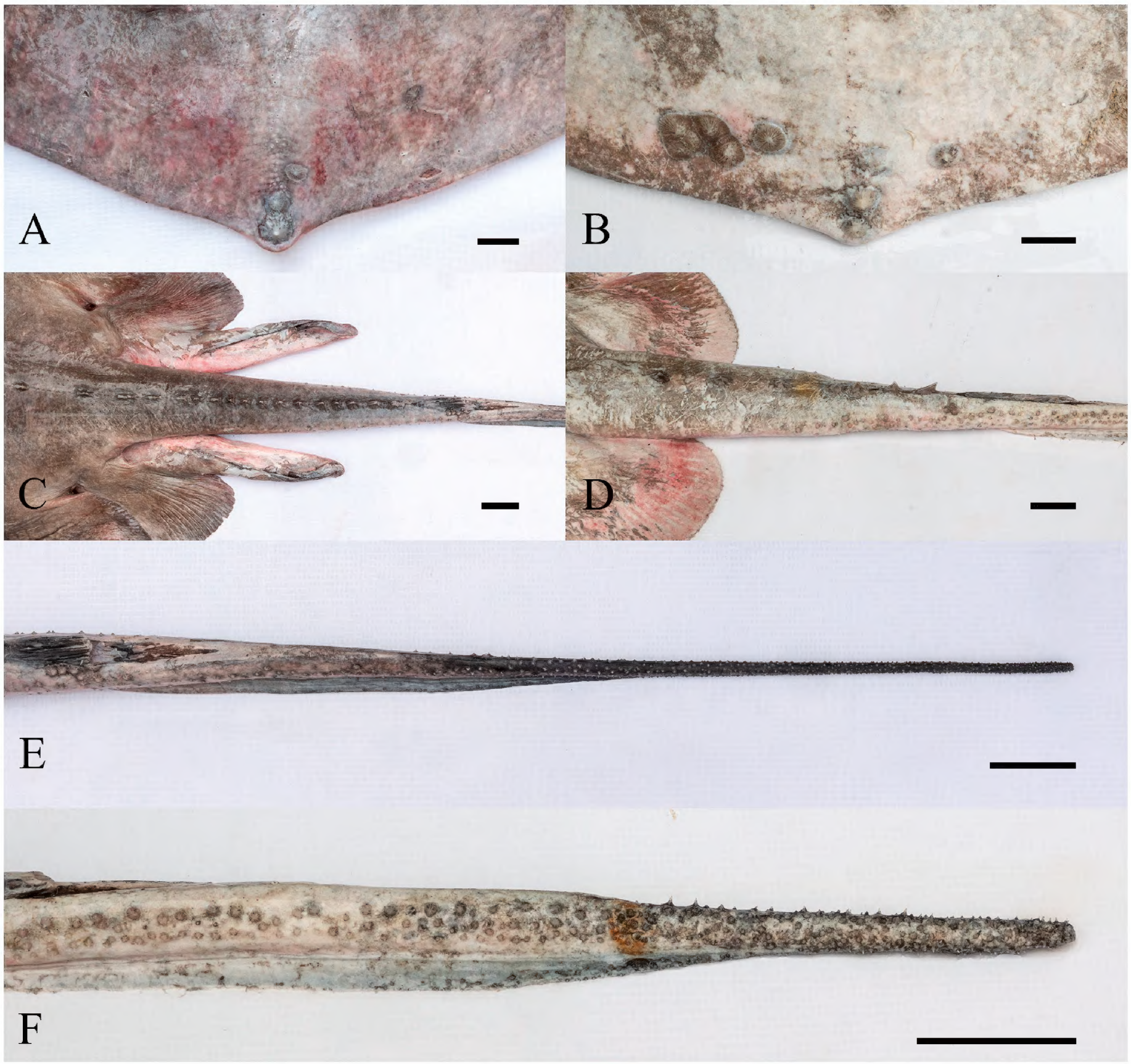

Figure 3. Morphological features of *Bathytoshia brevicaudata*: **A, B.** Ventral view of rostral region; **C, D.** Dorsal view of caudal peduncle base, with a pair of claspers on male; **E, F.** Lateral view of tail. Male (ZJOUMBM F00035: **A, C, E**); female (ECSFRI 28263: **B, D, F**). Scale bars: 2 cm (**A, B**); 5 cm (**C–F**), photo by Pan Liu.

Myliobatiform species (Fig. 6, Suppl. material 1: table S1). Each contained 37 mitochondrial genes (13 PCGs, 22 tRNAs, 2 rRNAs) and one control region, with all genes encoded on the H-chain except ND6 and eight tRNAs (trnS2, trnE, trnP, trnQ, trnA, trnN, trnC, trnY) on the L-chain (Fig. 6, Suppl. material 1: table S3). Three (PV699610) and four (PV699611) overlapping regions (1–10 bp) were identified, with the longest overlap (10 bp) at trnK-ATP8 in both mitogenomes. Fifteen gene spacers (1–36 bp) were present in each assembly, and the largest gap (1,896 bp) occurred between the control region and trnF (Suppl. material 1: table S3).

The overall base compositions of two *B. brevicaudata* mitogenomes (PV699610 and PV699611) were biased toward A and T at 59.2% (A = 30.8%, T = 28.4%, G = 13.5%, and C = 27.3%) with a positive A + T skew (PV699610: 0.041; PV699611: 0.040) and a negative G + C skew (PV699610: -0.340; PV699611: -0.339) (Suppl. material 1: table S4). Both mitogenomes exhibited a clear A + T preference, similar to other Dasyatinae fish (Suppl. material 1: table S1). The ATP8 gene had the highest A + T content (PV699610: 63.7%; PV699611: 63.1%), while the first codon position of the PCGs had the lowest (PV699610: 52.2%; PV699611: 52.1%) (Suppl. material 1: table S4).

Protein-coding mitochondrial genes and codon usage

The combined length of all protein-coding genes (PCGs) was 11,463 bp, with individual gene lengths ranging from 168 bp (*ATP8*) to 1,845 bp (*ND5*) (Suppl. material 1: table S4). All PCGs initiated with the canonical start codon ATG. Twelve PCGs possessed complete stop codons, while *ND4* terminated with an incomplete T stop codon (Suppl. material 1: table S3). AT-skew and GC-skew values for PCGs were consistently positive and negative, respectively (PV699610: AT-skew = 0.041, GC-skew = -0.340; PV699611:

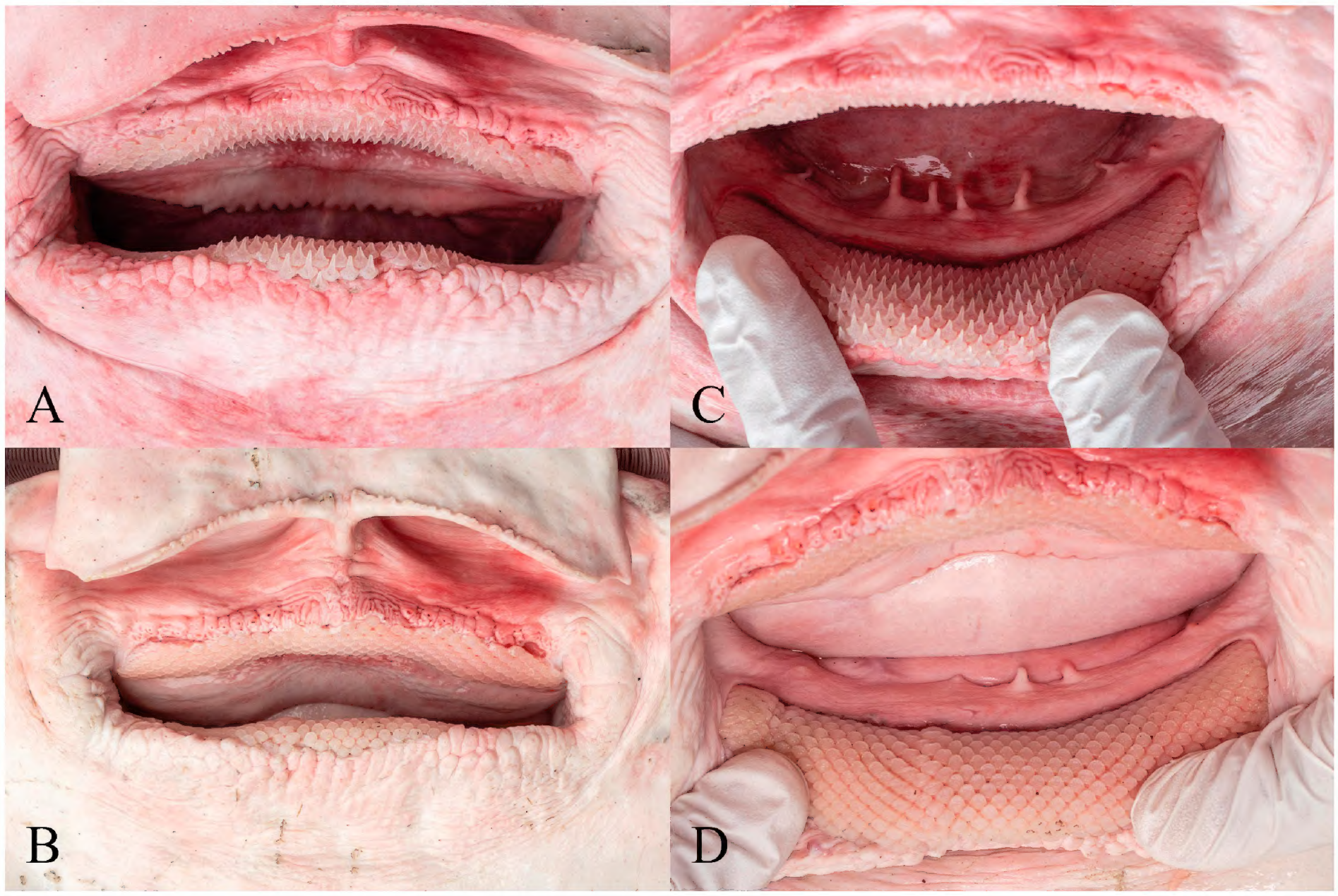

Figure 4. Dentition and oral papillae of *Bathytoshia brevicaudata*. **A, C.** Male specimen (ZJOUMBM F00035); **B, D.** Female specimen (ECSFRI 28263), photo by Pan Liu.

Figure 5. Stomach contents of *Bathytoshia brevicaudata* (female, ECSFRI 28263) and associated fishhooks. These contents are deposited at the SHNHM, preserved in 95% ethanol (SNHM-Hfi13442), photo by Pan Liu.

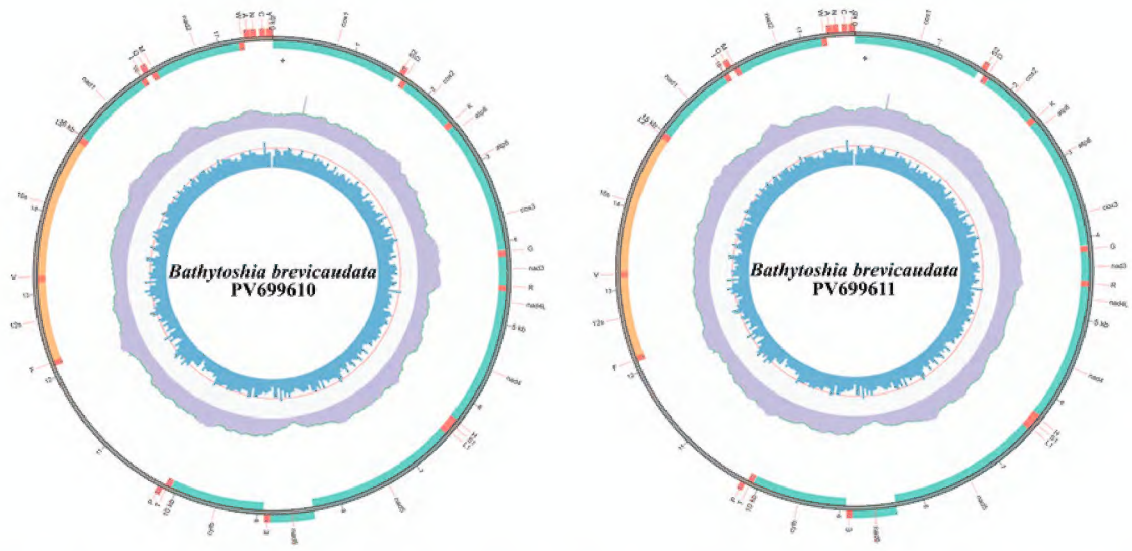

Figure 6. The complete mitogenome of *Bathytoshia brevicaudata*. The middle and innermost circles represent depth distribution and GC content, respectively. The outermost circle shows gene arrangements, with green for PCGs fragments, orange for rRNAs and red for tRNAs.

AT-skew = 0.040, GC-skew = -0.339; Suppl. material 1: table S4), indicating higher genomic abundances of adenine and cytosine relative to their complementary bases.

The amino acid usage and RSCU values in the PCGs of *B. brevicaudata* are summarized in Suppl. material 1: table S5, fig. S8. The mitogenome encoded a total of 3,821 amino acids, among which leucine (17.51%) and cysteine (0.60%) were the most and the least frequently used amino acids, respectively. The six most frequently used codons in *B. brevicaudata* were CUA(Leu), AUU(Ile), CUC(Leu), AUC(Ile), UUC(Phe), ACA(Thr).

Selection pressure analysis

To investigate the selective pressure on 13 PGCs of 17 Dasyatinae species, we calculated the non-synonymous substitutions rate (Ka) to the synonymous substitutions rate (Ks) ratio (Ka/Ks). The Ka/Ks ratios of all PCGs were far lower than one (Suppl. material 1: fig. S9). The *atp8* gene exhibited the highest ratio (Ka/Ks = 0.1903) of all the PCGs, whereas the *COX2* gene had the lowest ratio (Ka/Ks = 0.0302).

Transfer RNA and ribosomal RNA genes

The mitogenome of *B. brevicaudata* consisted of 22 tRNA genes individually ranging in size from 68 bp (trnS1) to 75 bp (trnL2) (Suppl. material 1: table S3), representing 8.83% (1557 bp) of the entire mitogenome (Suppl. material 1: table S4). Among the 22 tRNA genes, 14 tRNA genes were encoded on the H strand, while 8 tRNA genes were encoded on the L strand (Suppl. material 1: table S3). All tRNA genes were predicted to fold into the typical cloverleaf secondary structures except that the *trnS1* lacked the dihydrouridine (DHU) arm (Suppl. material 1: fig. S10). The 22 tRNA genes exhibited high A+T content in both strains (PV69960: 62.0%; PV69961: 61.7%). Both strains showed positive skew values: PV69960 had an A+T skew of +0.039 and a G+C skew of +0.069; PV69961 had an A+T skew of +0.047 and a G+C skew of +0.057 (Suppl. material 1: table S4).

The two rRNA genes, *12S* and *16S* rRNA genes, were 964 bp and 1,696 bp in length, respectively (Suppl. material 1: table S4). The rRNA genes were located between *trnF*(gaa) and *trnL*(uaa), separated from each other by *trnV*(uac) (Fig. 6, Suppl. material 1: table S3), as observed in other vertebrates. The two rRNA genes exhibited an A+T content of 56.4% and G+C content of 60.2% in PV69960 (G+C: 60.3% in PV69961). The 12S rRNA gene showed consistent positive A+T skew (+0.165) and negative G+C skew (-0.167) in both strains. For the 16S rRNA gene, PV69960 had an A+T skew of +0.162 and G+C skew of -0.108, while PV69961 showed values of +0.160 and -0.107, respectively (Suppl. material 1: table S4). These values indicate a clear bias in favor of the utilization of A and C nucleotides.

Genetic divergence among Bathytoshia species

The pairwise genetic p-distances within and among the three *Bathytoshia* species are summarized in Table 2.

Table 2. Genetic p-distances (Mean ± SD) among *Bathytoshia* species.

Comparison	COI (n; Mean ± SD)	ND2 (n; Mean ± SD)
Bb vs Bb	36; 0.0021 ± 0.0018	6; 0.0037 ± 0.0034
Bl vs Bl	225; 0.0831 ± 0.0870	-
Bc vs Bc	400; 0.0081 ± 0.0067	36; 0.0008 ± 0.0006
Bb vs Bc	147; 0.0375 ± 0.0026	28; 0.0522 ± 0.0008
Bb vs Bl	112; 0.0797 ± 0.0700	4; 0.0540 ± 0.0006
Bc vs Bl	336; 0.0620 ± 0.0788	7; 0.0059 ± 0.0007

Note: Species abbreviations: Bb, *Bathytoshia brevicaudata*; Bc, *Bathytoshia centroura*; Bl, *Bathytoshia lata*.

The analysis of mitochondrial p-distances revealed distinct patterns of genetic divergence within and among the three *Bathytoshia* species (Table 2). For the COI gene, intraspecific distances were lowest, averaging 0.0021 for *B. brevicaudata* (Bb), 0.0081 for *B. centroura* (Bc), and 0.0831 for *B. lata* (Bl). Interspecific distances were markedly higher, with the Bb-Bc comparison (0.0375) showing a clear separation, while distances involving *B. lata* were the greatest (Bb-Bl: 0.0797; Bc-Bl: 0.0620).

A similar trend was observed for the ND2 gene, where intraspecific distances for Bb and Bc were minimal (0.0037 and 0.0008, respectively). The interspecific

distance between Bb and Bc was substantially larger (0.0522), and comparisons involving *B. lata*, though based on limited data (n = 4–7), also showed significant divergence (Bb-Bl: 0.0540; Bc-Bl: 0.0059).

Phylogenetic analysis

The myliobatiform phylogeny reveals Aetobatidae as the earliest diverging lineage, followed by two primary clades: Clade I comprises a monophyletic Plesiobatidae + Urolophidae lineage embedding a sister group relationship between the monophyletic clades Rhinopteridae and Mobulidae, with the monophyletic clade Gymnuridae nested within; Clade II consists of a strongly monophyletic Potamotrygonidae (100% support) forming an independent branch, sister to the monophyletic clade Dasyatidae. Within Dasyatidae, Hypolophinae diverges first, followed by Urogymninae and Neotrygoninae, with Dasyatinae forming the most speciose clade. *Hypanus* Rafinesque, 1818 is monophyletic; *Dasyatis* Rafinesque, 1810 and *Taeniurops* Garman, 1913 form a sister clade; *Hemitrygon* Müller & Henle, 1838 is nested within *Telatrygon* Last, Naylor & Manjaji-Matsumoto, 2016; and *Pteroplatytrygon* Fowler, 1910 is nested within *Bathytoshia* Whitley, 1933 (Fig. 7). Phylogenetic analyses group mitochondrial sequences from our East China Sea specimens with conspecifics collected off waters of South Korea.

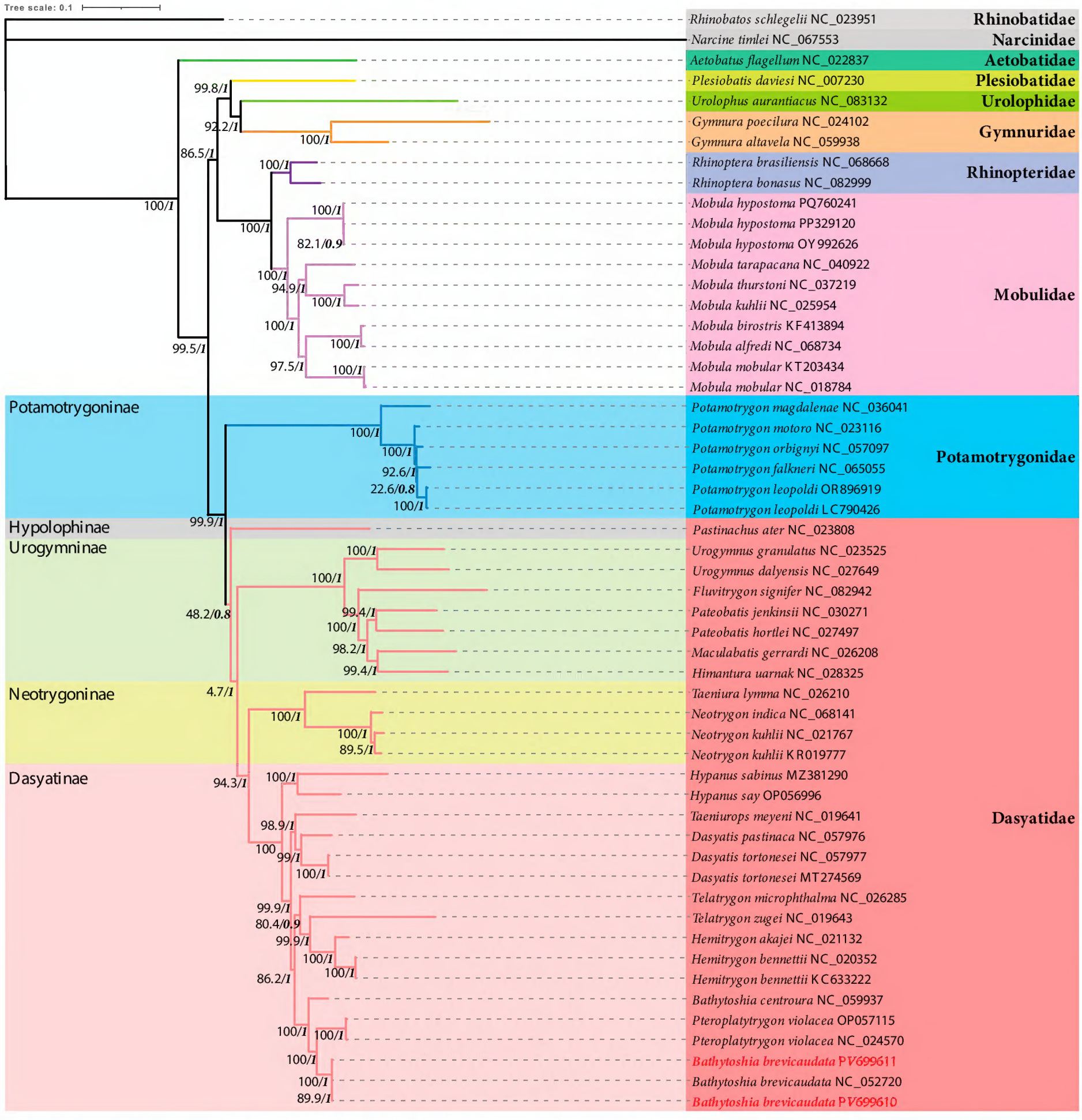

Figure 7. Phylogenetic reconstruction of Myliobatiformes inferred from 15 mitochondrial genes (13 protein-coding genes, two ribosomal RNAs) using Bayesian inference and maximum likelihood analyses. Numbers above branches indicate ML bootstrap and Bayesian posterior probabilities, respectively.

Discussion

Our study reveals previously underappreciated aspects of *Bathytoshia brevicaudata* biology, encompassing sexual dimorphism, trophic ecology, and migratory behavior, while also clarifying its phylogenetic position.

First, we identified significant sexual dimorphism in oral papilla counts and pharyngeal dentition. Diagnostically significant sexual dimorphism characterizes *B. brevicaudata*: Males possess seven oral papillae rows versus five in females, with female configurations corresponding to prior descriptions (Garrick 1954; Last and Stewart 2015) and male counts aligning with documented ranges (Last et al. 2016a, 2016b). The sexes also exhibit differences in the mid-dorsal tubercles, with mature males possessing nine such tubercles and females only three. Further dimorphism manifests in pharyngeal dentition—acute cusps in males versus bluntly rounded in females—potentially linked to seasonal mating adaptations rather than constitutive sexual disparity (Kajiura and Tricas 1996).

Our findings also revise the understanding of this species' dietary habits and provide evidence of large-scale movements. Stomach content analysis suggested that dietary composition of *B. brevicaudata* may shift with body size and geographic location. Contrary to the previous assertion that this species "feeds on invertebrates and small fishes" (Last et al. 2016b), stomach content analysis of a dissected female specimen (Fig. 5) revealed not only small teleosts but also a Horsehead Tilefish (*Branchiostegus japonicus*) exceeding 30 cm TL, indicating underestimated predatory capacity.

Furthermore, co-occurring anthropogenic markers—a coastal-origin J-hook (GP 15.2 mm) and a pelagic-origin circle hook (GP 12.4 mm) piercing the gastric wall—provide empirical evidence of transboundary movements between neritic and oceanic zones in the Western North Pacific. The dispersal of *B. brevicaudata* relies on shallow coastal waters above 250 m depth in temperate regions, while deep oceanic basins and excessively warm tropical waters restrict the movement of this species (Le Port and Lavery 2012). The northern East China Sea connects to the Sea of Japan via the Tsushima Strait, and the entire area features a continuous continental shelf beneath the sea surface. In early Spring, the powerful cold water from the northern basin of the Tsushima Strait spills through the southern gap of the Oki Spur, forming a cold water area distinctly different from the warm upper-layer Tsushima Warm Current (Senjyu et al. 2025), thereby facilitating the southward dispersal of Short-tail Stingrays.

Typically, female individuals of *B. brevicaudata* exhibit greater fidelity to breeding sites and generally disperse over shorter distances compared to males (Le Port and Lavery 2012). Based on this inference, the relatively sharper teeth of male individuals may also function to more effectively capture relatively agile and fast-swimming prey during long-distance dispersal. This could reflect an adaptive specialization for long-range migration. Although further evidence is required for verification, we can speculate that the capture of one adult female among the two specimens collected this time may indicate that some female individuals are beginning to attempt settlement in the northern East China Sea. It is plausible that, aided by the relatively cold bottom water masses in this area, they are gradually attempting to establish breeding grounds here.

The complete mitogenomes of the female (PV699610) and male (PV699611) *Bathytoshia brevicaudata* were identical in length (17,640 bp) and shared a highly conserved structure, with the same 37 genes and control region (Suppl. material 1: tables S1, S3, Fig. 6). Minor differences, such as the number of overlapping regions (3 in female vs. 4 in male), did not affect key features like the longest *trnK-ATP8* overlap or the overall A+T content (59.2%) and nucleotide skews, which were nearly identical (Suppl. material 1: tables S3, S4). This conservation extended to all protein-coding genes, which had identical lengths, uniform start/stop codons, and highly similar codon usage patterns (Suppl. material 1: table S5), as well as to the tRNA and rRNA genes. The remarkable consistency across all genomic features indicates a strong functional constraint on the mitochondrial genome of *B. brevicaudata*.

In our research, phylogenetic reconstruction based on 15 mitochondrial genes demonstrates that the genus *Pteroplatytrygon* is nested within the genus *Bathytoshia*, which suggests that the genus *Bathytoshia* is not monophyletic. This result markedly contrasts with the previous COI-based phylogenetic reconstruction, which recovered the two genera as sister groups (Ryo et al. 2020). While previous studies relied solely on COI sequences, our current investigation integrates both COI and ND2 sequences for analysis. The differences in methodological approaches may partially explain the discrepancies in conclusions. However, our study further reveals a close evolutionary relationship between the genera *Bathytoshia* and *Pteroplatytrygon*. Although the species of these two genera are highly divergent in their ecological niches, they share common morphological characteristics such as a well-developed ventral tail fold, a robust trunk, a small orbit diameter, and a broad nasal curtain. The morphological similarities, combined with molecular evidence, suggest that the genus *Pteroplatytrygon* may represent a highly specialized lineage within the genus *Bathytoshia* that has adapted to the oceanic pelagic zone. However, the evolutionary relationship between these two genera remains to be further investigated and clarified.

Our genetic analyses provide high-resolution phylogenetic insights and reveal unexpected intraspecific diversity within the genus. Phylogenetic reconstruction using complete mitogenomes provides greater resolution for interspecific relationships than fragmentary COI data. Our mitogenomic phylogeny reveals distinctions between *Mobula alfredi* (Krefft, 1868) and

M. birostris (Walbaum, 1792)—aligned with Poortvliet et al. (2015) who placed these species as sisters based on *cox1*, *nad5*, and *rag1* sequences. Despite their similar branch lengths, the 96.73% mitogenomic distance confirms species-level divergence. Conversely, sequences NC_018784 (annotated as *Mobula japanica* (Müller & Henle, 1841)) and KT203434 (*M. mobular* Bonnaterre, 1788) show 98.74% whole-mitogenome identity, indicating conspecificity—confirming White et al. (2018)'s taxonomic revision.

Our analysis of mitochondrial p-distances provides critical quantitative insights that both corroborate and refine the phylogenetic relationships suggested by Naylor et al. (2012). The clear genetic boundaries distinguishing *Bathytoshia brevicaudata* from other species in *Bathytoshia* strongly support its treatment as a distinct species, a finding consistent with its morphological delineation.

Notably, our results offer a genetic perspective on the close relationship between *B. brevicaudata* and *B. centroura* first proposed by Naylor et al. (2012), who noted that these species grouped closely based on a single specimen of *B. brevicaudata*. Our data, derived from multiple individuals, robustly confirms this sister-species relationship. The genetic distances (p-distances) provide preliminary evidence for the phylogenetic structure within the genus. The smallest distance was observed between *B. brevicaudata* and *B. centroura* (0.0375), which was substantially lower than their distances to *B. lata* (0.0797 and 0.0620, respectively). This pattern is consistent with a clade comprising *B. brevicaudata* and *B. centroura*. Historically, the genus *Bathytoshia* was long classified under the genus *Dasyatis*, until it was formally recognized as a distinct genus following the systematic revision and splitting of the genus *Dasyatis* (Naylor et al. 2012). This pattern validates the taxonomic revision that grouped these species into the resurrected genus *Bathytoshia*, resolving the historical placement instability noted by Naylor et al. (2012) for related forms.

Moreover, the comparison of the two specimens collected this time with the *B. brevicaudata* specimen (NC_052720) collected from South Korean waters in terms of COI (0) and ND2 (0.001010101) revealed minimal differentiation, indicating that they belong to the same population.

Long-distance dispersal is not unique to *B. brevicaudata*. Its congener, *B.lata*, has also demonstrated remarkable migratory abilities, with its distribution in the Northwestern Pacific expanding northward to areas such as Kochi, Mie, and Chiba Prefectures (Japan), and it appears to be dispersing along the flow paths of the Kuroshio Current or the Tsushima Current (Ryo et al. 2020; Hata et al. 2022). The dispersal capacity of large stingrays may have been previously underestimated. In this process, ocean currents could act as highways, further facilitating distribution range expansion. Additionally, cold-water masses trapped in deep-water regions may create pathways for the dispersal of cartilaginous fishes. The southward and northward expansion of cartilaginous fishes could be far more common than previously thought, and in the context of climate change, this is a research topic worthy of attention.

Furthermore, our study reveals a significant and unexpected finding: an exceptionally high intraspecific p-distance within *B. lata* (0.0831). Among which, the maximum P-distance (0.180579) was observed between sample FJ583341_1 (from Sri Lanka) and HQ945977_1 (from Spain). Samples collected from India and Sri Lanka exhibit remarkable genetic differences compared to populations in other seas, indicating they could be a unique evolutionary clade. This value is not only an order of magnitude greater than that of its congeners but also exceeds many of the interspecific distances within the genus. However, this conclusion requires further validation through examination of local voucher specimens.

Our research may provide new insights into the dispersal pathways of the Short-tailed Stingray, as this species' migratory capacity could be far greater than previously recognized. Moreover, our genetic divergence data solidify the framework of the genus *Bathytoshia* and highlight the power of comprehensive sampling. By quantifying the genetic relationships hinted at in earlier works, this study provides a solid molecular foundation for the systematics of this group and identifies a critical avenue for future research.

Conclusion

This study provides the first records of *B. brevicaudata* from the East China Sea and provides detailed records of its morphological characteristics and sexual dimorphism. Diagnostic features, including the distinctive white pores distributed around the side of the head and anterior disc, combined with the relatively short tail, confirm its identity as *B. brevicaudata*, which expands its known distribution in the Western Pacific and contributes a new species to the recorded chondrichthyan fauna of China.

Beyond taxonomy, our integrated analyses revealed pronounced sexual dimorphism in oral papillae, dorsal tubercles, and dentition. Dietary examination further identified large teleosts (>30 cm TL) as prey, revising previous ecological assumptions, while the co-occurrence of coastal and pelagic fishing hook types provides empirical evidence of transboundary movements. The complete mitogenome assemblies exhibited structural conservation and strong purifying selection, consistent with typical dasyatid genomic traits. Collectively, these findings significantly enhance the species characterization, rectify prior underestimations of its ecology, and underscore the need for cross-jurisdictional management strategies.

Funding

National Key R&D Program of China (2024YFD2400401).

Author contributions

Jia-Jie Chen conducted morphometric analyses, molecular experiments, and manuscript preparation, with specific responsibility for standardized measurement protocols and methodological schematization. Jiang-Yuan Chen performed specimen collection, taxonomic identification, and preliminary morphological descriptions. Pan Liu and Xing-Le Guo executed photographic documentation and specimen measurements. Shen Zeng and De-Yuan Yang carried out mitogenome annotation, assembly, and phylogenetic reconstruction. Wen-Hong Fang and Jian Chen oversaw research design and funding acquisition. Jun-Sheng Zhong and Shen-Long Zhao provided external scientific guidance. Wen-Hong Fang and Pan Liu supervised project coordination and funding administration. Jia-Jie Chen and Jiang-Yuan Chen contributed equally as co-first authors. All authors critically reviewed and approved the final manuscript.

Acknowledgements

We are grateful to Mr. Huai-Ying Sun for technical assistance during specimen dissection, and to Mr. Rui-Lin Huang for his support in photographic documentation. We also extend our thanks to Hai-Shui Lin of Shanghai Majorbio Bio-pharm Biotechnology Co., Ltd. (Shanghai, China) for sequencing services, and Researcher Han-Ye Zhang (East China Sea Fisheries Research Institute) for scientific guidance. Finally, we acknowledge the editors and anonymous reviewers for their constructive comments, which greatly improved the quality of this manuscript.

References

Alós J (2008) Influence of anatomical hooking depth, capture depth, and venting on mortality of painted comber (Serranus scriba) released by recreational anglers. ICES Journal of Marine Science 65: 1620–1625. https://doi.org/10.1093/icesjms/fsn151

Bernt M, Donath A, Jühling F, Externbrink F, Florentz C, Fritzsch G, Pütz J, Middendorf M, Stadler PF (2013) MITOS: Improved de novo metazoan mitochondrial genome annotation. Molecular Phylogenetics and Evolution 69: 313–319. https://doi.org/10.1016/j.ympev.2012.08.023

Castresana J (2000) Selection of conserved blocks from multiple alignments for their use in phylogenetic analysis. Molecular Biology and Evolution 17: 540–552. https://doi.org/10.1093/oxfordjournals.molbev.a026334

Chen J, Wang X, Zeng S, Tian W, Yang D, Ye J, Zhong J, Jiang C (2024) Morphometric and phylogenetic analysis of a commercial fish Leiognathus equula (Teleostei, Leiognathidae). ZooKeys 1219: 249–270. https://doi.org/10.3897/zookeys.1219.130546

Chan PP, Lin BY, Mak AJ, Lowe TM (2021) tRNAscan-SE 2.0: Improved detection and functional classification of transfer RNA genes. Nucleic Acids Research 49: 9077–9096. https://doi.org/10.1093/nar/gkab688

Chen S, Zhou Y, Chen Y, Gu J (2018) fastp: An ultra-fast all-in-one FASTQ preprocessor. Bioinformatics 34: i884–i890. https://doi.org/10.1093/bioinformatics/bty560

Compagno LJV, Roberts TR (1982) Freshwater stingrays (Dasyatidae) of Southeast Asia and New Guinea, with description of a new species of Hirnantura and reports of unidentified species. Environmental Biology of Fishes 7: 321–339. https://doi.org/10.1007/BF00005567

Dierckxsens N, Mardulyn P, Smits G (2017) NOVOPlasty: *De novo* assembly of organelle genomes from whole genome data. Nucleic Acids Research 45: e18. https://doi.org/10.1093/nar/gkw955

Donath A, Jühling F, Al-Arab M, Bernhart SH, Reinhardt F, Stadler PF, Middendorf M, Bernt M (2019) Improved annotation of protein-coding genes boundaries in metazoan mitochondrial genomes. Nucleic Acids Research 47: 10543–10552. https://doi.org/10.1093/nar/gkz833

Garrick JAF (1954) Studies on New Zealand Elasmobranchii. Part II. A description of Dasyatis brevicaudatus (Hutton), Batoidei, with a review of records of the species outside New Zealand. Transactions of the Royal Society of New Zealand 81: 189–198.

Hata H, Lavoué S, Motomura H (2022) Description of three new species previously identified as Stolephorus bengalensis (Dutt & Babu Rao, 1959) or Stolephorus insularis Hardenberg, 1933 and a re-description of S. bengalensis (Chordata, Osteichthyes, Clupeiformes, Engraulidae). ZooKeys 1121: 145–173. https://doi.org/10.3897/zookeys.1121.84171

Hutton FW (1875) Descriptions of new species of New-Zealand fish. Annals and Magazine of Natural History (Series 4) 16: 313–317. https://doi.org/10.1080/00222937508681859

Jin J-J, Yu W-B, Yang J-B, Song Y, dePamphilis CW, Yi T-S, Li D-Z (2020) GetOrganelle: A fast and versatile toolkit for accurate de novo assembly of organelle genomes. Genome Biology 21: 241. https://doi.org/10.1186/s13059-020-02154-5

Kajiura SM, Tricas TC (1996) Seasonal Dynamics of Dental Sexual Dimorphism in the Atlantic Stingray *Dasyatis Sabina*. The Journal of Experimental Biology 199: 2297–2306. https://doi.org/10.1242/jeb.199.10.2297

Kalyaanamoorthy S, Minh BQ, Wong TKF, Von Haeseler A, Jermiin LS (2017) ModelFinder: Fast model selection for accurate phylogenetic estimates. Nature Methods 14: 587–589. https://doi.org/10.1038/nmeth.4285

Katoh K, Standley DM (2013) MAFFT Multiple sequence alignment software version 7: Improvements in performance and usability. Molecular Biology and Evolution 30: 772–780. https://doi.org/10.1093/molbev/mst010

Kerpedjiev P, Hammer S, Hofacker IL (2015) Forna (force-directed RNA): Simple and effective online RNA secondary structure diagrams. Bioinformatics 31: 3377–3379. https://doi.org/10.1093/bioinformatics/btv372

Kim J-O, Seo YB, Shin J, Yang J-Y, Kim G-D (2020) The complete mitochondrial genome of pitted stingray *Bathytoshia brevicaudata* (Myliobatiformes: Dasyatoidea). Mitochondrial DNA. Part B, Resources 5: 3538–3539. https://doi.org/10.1080/23802359.2020.1829121

Kumar S, Stecher G, Li M, Knyaz C, Tamura K (2018) MEGA X: Molecular evolutionary genetics analysis across computing platforms. Molecular Biology and Evolution 35: 1547–1549. https://doi.org/10.1093/molbev/msy096

Last PR, Stewart AL (2015) 33 Family Dasyatidae. In: Roberts CD, Stewart AL, Struthers CD (Eds) The fishes of New Zealand. Vol. 2. Systematic Accounts. Te Papa Press, Wellington, 198 pp.

Last PR, Naylor GJP, Manjaji-Matsumoto BM (2016a) A revised classification of the family Dasyatidae (Chondrichthyes: Myliobatiformes) based on new morphological and molecular insights. Zootaxa 4139(3): 345–368. https://doi.org/10.11646/zootaxa.4139.3.2

Last PR, Manjaji-Matsumoto BM, Naylor GJP, White WT (2016b) 25. Stingrays. Family Dasyatidae. In: Last PR, Manjaji-Matsumoto BM, Naylor GJP, White WT (Eds) Rays of the World. CSIRO Publishing, Comstock Publishing Associates, 790 pp. https://doi.org/10.1071/9780643109148-ch25

Le Port A, Lavery S (2012) Population structure and phylogeography of the short-tailed stingray, *Dasyatis brevicaudata* (Hutton 1875), in the Southern Hemisphere. The Journal of Heredity 103: 174–185. https://doi.org/10.1093/jhered/esr131

Le Port A, Pawley M, Lavery S (2013) Speciation of two stingrays with antitropical distributions: Low levels of divergence in mitochondrial DNA and morphological characters suggest recent evolution. Aquatic Biology 19: 153–165. https://doi.org/10.3354/ab00518

Letunic I, Bork P (2016) Interactive tree of life (iTOL) v3: An online tool for the display and annotation of phylogenetic and other trees. Nucleic Acids Research 44: W242–W245. https://doi.org/10.1093/nar/gkw290

Lowe TM, Chan PP (2016) tRNAscan-SE On-line: Integrating search and context for analysis of transfer RNA genes. Nucleic Acids Research 44: W54–W57. https://doi.org/10.1093/nar/gkw413

Meng G, Li Y, Yang C, Liu S (2019) MitoZ: A toolkit for animal mitochondrial genome assembly, annotation and visualization. Nucleic Acids Research 47: e63–e63. https://doi.org/10.1093/nar/gkz173

Miyosi Y (1939) Description of three new species of Elasmobranchiate fishes collected at Hyuga Nada, Japan. Bulletin of the Biogeographical Society Tokyo 9: 91–97.

Naylor GJP, Caira JN, Jensen K (2012) A DNA sequence–based approach to the identification of shark and ray species and its implications for global elasmobranch diversity and parasitology. Bulletin of the American Museum of Natural History 367: 1–262. https://doi.org/10.1206/754.1

Perna NT, Kocher TD (1995) Patterns of nueleotide composition at fourfold degenerate sites of animal mitochondrial genomes. Journal of Molecular Evolution 41: 353–358. https://doi.org/10.1007/BF01215182

Poortvliet M, Olsen JL, Croll DA, Bernardi G, Newton K, Kollias S, O'Sullivan J, Fernando D, Stevens G, Galván Magaña F, Seret B, Wintner S, Hoarau G (2015) A dated molecular phylogeny of manta and devil rays (Mobulidae) based on mitogenome and nuclear sequences. Molecular Phylogenetics and Evolution 83: 72–85. https://doi.org/10.1016/j.ympev.2014.10.012

Ronquist F, Teslenko M, Van Der Mark P, Ayres DL, Darling A, Höhna S, Larget B, Liu L, Suchard MA, Huelsenbeck JP (2012) MrBayes 3.2: Efficient Bayesian Phylogenetic Inference and Model Choice Across a Large Model Space. Systematic Biology 61: 539–542. https://doi.org/10.1093/sysbio/sys029

Rozas J, Ferrer-Mata A, Sánchez-DelBarrio JC, Guirao-Rico S, Librado P, Ramos-Onsins SE, Sánchez-Gracia A (2017) DnaSP 6: DNA Sequence Polymorphism Analysis of Large Data Sets. Molecular Biology and Evolution 34: 3299–3302. https://doi.org/10.1093/molbev/msx248

Ryo M, Yoshikazu K, Kiyonori N, Yoshitsugu K, Hiromitsu E, Yoshiaki K (2020) Records of the Brown Stingray Bathytoshia lata from Kochi and Mie Prefectures, Japan, with comments on their morphological and genetic characteristics. Nihon Seibutsu Chiri Gakkai Kaiho 75: 31–40.

Senjyu T, Tanimura S, Aramaki T (2025) Deep water overflow through the southern gap of the Oki Spur in the Japan Sea. Deep-sea Research. Part I, Oceanographic Research Papers 225: 104578. https://doi.org/10.1016/j.dsr.2025.104578

Swimmer Y, Arauz R, Wang J, Suter J, Musyl M, Bolaños A, López A (2010) Comparing the effects of offset and non-offset circle hooks on catch rates of fish and sea turtles in a shallow longline fishery. Aquatic Conservation 20: 445–451. https://doi.org/10.1002/aqc.1108

Takushi Y, Itou M, Yamada M, Motomura H (2025) First records of 62 fish species from the western and southern coasts of Satsuma Peninsula, Kagoshima Prefecture, Kyushu, Japan. Ichthy, Natural History of Fishes of Japan. https://doi.org/10.34583/ichthy.53.0_23

White WT, Corrigan S, Yang L, Henderson AC, Bazinet AL, Swofford DL, Naylor GJP (2018) Phylogeny of the manta and devilrays (Chondrichthyes: mobulidae), with an updated taxonomic arrangement for the family. Zoological Journal of the Linnean Society 182: 50–75. https://doi.org/10.1093/zoolinnean/zlx018

Wu HL, Zhong JS (2021) Key to Marine and Estuarial Fishes of China. China Agriculture Press, Beijing, 1437 pp.

Xu Y, Zeng S, Meng Y, Yang D, Yang S (2024) The mitochondrial genome of *Hua aristarchorum* (Heude, 1889) (Gastropoda, Cerithioidea, Semisulcospiridae) and its phylogenetic implications. ZooKeys 1192: 237–255. https://doi.org/10.3897/zookeys.1192.116269

Yang D, Zeng S, Wang Z, Zhang Y, Yang D, Glasby CJ, Hwang J, Cai L (2024) Molecular systematics of Perinereis and an investigation of the status and relationships of the cultured species *Perinereis wilsoni* Glasby & Hsieh, 2006 (Annelida, Nereididae). Zoosystematics and Evolution 100(4): 1297–1314. https://doi.org/10.3897/zse.100.127201

Zhang D, Gao F, Jakovlić I, Zou H, Zhang J, Li WX, Wang GT (2020) PhyloSuite: An integrated and scalable desktop platform for streamlined molecular sequence data management and evolutionary phylogenetics studies. Molecular Ecology Resources 20: 348–355. https://doi.org/10.1111/1755-0998.13096

Zhu YD, Meng QW (2001) Fauna Sinica, Cyclostomata, Chondrichthyes. Science Press, Beijing, 552 pp.

Supplementary material 1

Supplementary information

Authors: Jia-Jie Chen, Jiang-Yuan Chen, Xing-Le Guo, Sheng Zeng, De-Yuan Yang, Jun-Sheng Zhong, Shen-Long Zhao, Wen-Hong Fang, Jian Chen, Pan Liu

Data type: zip

Explanation note: **table S1.** Mitochondrial sequences used in the phylogenetic analysis as shown in this study. **table S2.** Best partitioning schemes and models based on different datasets for Bayesian inference (BI) and maximum likelihood (ML) analysis. **table S3.** Information on each gene fragment of *B. brevicaudata*. **table S4.** Base composition of the *B. brevicaudata* mitochondrial genome. **table S5.** Codon number and RSCU of *B. brevicaudata* mitochondrial PCGs. **table S6.** p-distance matrices of COI and ND2 genes for three *Bathytoshia* species. **figure S1.** *B. lata* landed at a fishing pier in Songmen Town, Taizhou City, Zhejiang Province, China, these stingrays were caught in the outer edge of the continental shelf of the East China Sea, photographed April 2024. Photo by Jiang-Yuan Chen. **figure S2.** *B. lata* found in the Gaoqi wholesale fish market in Xiamen, Fujian Province, photographed January 2025, these individuals were reported to have been caught from the southern part of the Taiwan Strait to the Dongsha Islands. Photo by Jiang-Yuan Chen. **figure S3.** *B. brevicaudata* (voucher no. ZJOUMBM F00035) was photographed in situ at Songmen Fishing Pier, Zhejiang Province, China, on 1 March 2025, with photographic documentation by Mr. Zhi-Fu Liang. **figure S4.** *B. brevicaudata* (voucher no. ECSFRI 28263) was photographed in situ at Songmen Fishing Pier, Zhejiang Province, China, on 26 March 2025, withscreenshots from the video provided by Hui-Sen Li. **figure S5.** Dorsal (A) and ventral (B) views of claspers in the matured male *B. brevicaudata* (voucher no. ZJOUMBM F00035). Photo by Xing-Le Guo. **figure S6.** Fishhook penetrating the gastric wall into the liver of *B. brevicaudata*, photo by Pan Liu. **figure S7.** The liver (above) and stomach (below) of *B. brevicaudata* (ECSFRI 28366~28367). **figure S8.** Relative synonymous codon usage of all PCGs in the mitogenome of *B. brevicaudata*. **figure S9.** The Ka, Ks, and Ka/Ks values for each PCG from 17 Dasyatinae sequence in Table 1. **figure S10.** Secondary structure of the 22 tRNA genes of the mitochondrial genome of *E. melanoptera*.

Copyright notice: This dataset is made available under the Open Database License (http://opendatacommons.org/licenses/odbl/1.0/). The Open Database License (ODbL) is a license agreement intended to allow users to freely share, modify, and use this Dataset while maintaining this same freedom for others, provided that the original source and author(s) are credited.

Link: https://doi.org/10.3897/zse.101.164102.suppl1